

Direct observation of shock-induced phase transformation in polycrystalline iron via *in situ* x-ray diffraction

Fan Zhang(张帆), Jia-Qin Dong(董佳钦), Zhi-Yong Xie(谢志勇), Zhi-Yu He(贺芝宇), Hua Shu(舒桦), Rui-Rong Wang(王瑞荣), Jun Xiong(熊俊), Guo Jia(贾果), Zhi-Heng Fang(方智恒), Wei Wang(王伟), Da-Du Xiao(肖大武), An-Le Lei(雷安乐), Jie Chen(陈洁), and Xiu-Guang Huang(黄秀光)

Citation: Chin. Phys. B, 2024, 33 (**10**): 106101. DOI: 10.1088/1674-1056/ad625a
Journal homepage: http://cpb.iphy.ac.cn; http://iopscience.iop.org/cpb

What follows is a list of articles you may be interested in

Pressure-induced structural, electronic, and superconducting phase transitions in $TaSe_3$

Yuhang Li(李宇航), Pei Zhou(周佩), Chi Ding(丁驰), Qing Lu(鲁清), Xiaomeng Wang(王晓梦), and Jian Sun(孙建)
Chin. Phys. B, 2024, 33 (**10**): 106102. DOI: 10.1088/1674-1056/ad6f92

First-principles study of structural and electronic properties of multiferroic oxide Mn_3TeO_6 under high pressure

Xiao-Long Pan(潘小龙), Hao Wang(王豪), Lei Liu(柳雷), Xiang-Rong Chen(陈向荣), and Hua-Yun Geng(耿华运)
Chin. Phys. B, 2024, 33 (**7**): 076102. DOI: 10.1088/1674-1056/ad3ef6

Linear magnetoresistance and structural distortion in layered $SrCu_{4-x}P_2$ single crystals

Yong Nie(聂勇), Zheng Chen(陈正), Wensen Wei(韦文森), Huijie Li(李慧杰), Yong Zhang(张勇), Ming Mei(梅明), Yuanyuan Wang(王园园), Wenhai Song(宋文海), Dongsheng Song(宋东升), Zhaosheng Wang(王钊胜), Xiangde Zhu(朱相德), Wei Ning(宁伟), and Mingliang Tian(田明亮)
Chin. Phys. B, 2024, 33 (**1**): 016108. DOI: 10.1088/1674-1056/acf705

Ultrafast dynamics in photo-excited Mott insulator $Sr_3Ir_2O_7$ at high pressure

Xia Yin(尹霞), Jianbo Zhang(张建波), Wang Dong(王东), Takeshi Nakagawa, Chunsheng Xia(夏春生), Caoshun Zhang(张曹顺), Weicheng Guo(郭伟程), Jun Chang(昌峻), and Yang Ding(丁阳)
Chin. Phys. B, 2024, 33 (**1**): 016103. DOI: 10.1088/1674-1056/acdc8c

Classification and structural characteristics of amorphous materials based on interpretable deep learning

Jiamei Cui(崔佳梅), Yunjie Li(李韵洁), Cai Zhao(赵偲), and Wen Zheng(郑文)
Chin. Phys. B, 2023, 32 (**9**): 096101. DOI: 10.1088/1674-1056/acd7d0

Direct observation of shock-induced phase transformation in polycrystalline iron via *in situ* x-ray diffraction

Fan Zhang(张帆)[1,2,†], Jia-Qin Dong(董佳钦)[2], Zhi-Yong Xie(谢志勇)[2], Zhi-Yu He(贺芝宇)[2], Hua Shu(舒桦)[2], Rui-Rong Wang(王瑞荣)[2], Jun Xiong(熊俊)[2], Guo Jia(贾果)[2], Zhi-Heng Fang(方智恒)[2], Wei Wang(王伟)[2], Da-Wu Xiao(肖大武)[3], An-Le Lei(雷安乐)[2], Jie Chen(陈洁)[1], and Xiu-Guang Huang(黄秀光)[2,‡]

[1] *Collaborative Innovation Center of IFSA (CICIFSA), School of Physics and Astronomy, Center for Ultrafast Science and Technology, Key Laboratory for Laser Plasmas (Ministry of Education), Shanghai Jiao Tong University, Shanghai* 200240, *China*

[2] *Shanghai Institute of Laser Plasma, China Academy of Engineering Physics, Shanghai* 201800, *China*

[3] *Institute of Materials, China Academy of Engineering Physics, Mianyang* 621700, *China*

(Received 21 March 2024; revised manuscript received 4 June 2024; accepted manuscript online 12 July 2024)

Phase transition of polycrystalline iron compressed along the Hugoniot is studied by combining laser-driven shock with *in situ* x-ray diffraction technique. It is suggested that polycrystalline iron changes from an initial body-centered cubic structure to a hexagonal close-packed structure with increasing pressure (i.e., a phase transition from α to ε). The relationship between density and pressure for polycrystalline iron obtained from the present experiments is found to be in good agreement with the gas-gun Hugoniot data. Our results show that experiments with samples at lower temperatures under static loading, such as in a diamond anvil cell, lead to higher densities measured than those found under dynamic loading. This means that extrapolating results of static experiments may not predict the dynamic responses of materials accurately. In addition, neither the face-centered cubic structure seen in previous molecular-dynamics simulations or two-phase coexistence are found within our experimental pressure range.

Keywords: *in situ* x-ray diffraction, phase transition, polycrystalline iron

PACS: 61.05.cp, 64.70.K, 62.50.–p **DOI:** 10.1088/1674-1056/ad625a

1. Introduction

Iron is the most important and widely used metal material in modern industry, and it is also the main constituent element of the earth's solid core and outer molten core.[1–3] Examining iron's crystal structure and its phase transitions under high temperatures and pressures is important for understanding its physical properties and for constructing and verifying a multiphase equation of state (EOS) under extreme conditions,[4–6] which has great research value in fields including materials science,[7,8] geophysics,[9–11] and national defense engineering.[12,13]

In the 1950s, based on wave-profile analysis, Bancroft *et al.*[14] proposed that iron may undergo a shock-induced phase transition when the pressure is greater than 13 GPa. Subsequently, a series of experimental studies on the pressure-induced phase transition of iron were carried out using static[15–18] and dynamic loading techniques.[19–22] However, the solid-solid phase transitions of iron in the pressure range 10–30 GPa, especially under dynamic loading, are still not well understood; this includes obtaining the initial pressure of the phase transition, the time of phase nucleation, and the pressure span of the phase transition (i.e., the region of coexistence of two phases). The strain rate of dynamic loading is different from that of static pressure, and the strain-rate spans between different loading methods can be very large. For example, the strain-rate differences between loading techniques such as the Hopkinson pressure bar, gas guns, explosions, and high-power lasers can reach at least six orders of magnitude.[23] However, dynamic loading experiments are usually single shots, and their durations can be very short; as such, the internal structure of a sample is generally analyzed using wave-profile analysis of the free-surface velocity or particle velocity.[24,25] This does not allow for real-time and *in situ* observations of the microstructure during the experiments like those in the static experiments.[26,27]

In 2005, Kalantar *et al.*[28] used quasi-monochromatic x-rays generated by laser illumination of foils to investigate dynamic response characteristics of single-crystal iron under laser-induced shocks. They directly observed the phase transition from body-centered cubic (bcc) to hexagonal close-packed (hcp) of single-crystal iron at the atomic level for the first time. After that, Hawreliak *et al.*[29] studied the phase transformation of laser-shock-compressed polycrystalline iron using *in situ* x-ray diffraction, and they measured the value of the c/a ratio in the hcp phase. However, due to the relatively short development time of *in situ* x-ray diffraction diagnostic technology, the experimental work related to this aspect is not highly detailed, and many experimental results are not consistent with each other. For example, Li *et al.*[30] suggested that single-crystal iron maintains a bcc crystal structure up to

[†]Corresponding author. E-mail: zhang_fan@sjtu.edu.cn
[‡]Corresponding author. E-mail: huangxiuguang@sohu.com

© 2024 Chinese Physical Society and IOP Publishing Ltd

26 GPa, but in the work of Kalantar *et al.*,[28] single-crystal iron was found to have already undergone the phase transition at the same pressure. Hawreliak *et al.* showed that the there is still two-phase coexistence in polycrystalline iron under pressures greater than 20 GPa, which is somewhat different from the pressure range of two-phase coexistence established in the previous experiments.[31,32] In addition, some numerical simulations have predicted the presence of a face-centered cubic (fcc) phase during shock loading,[33] but such a structure has not been found in relevant experiments.[28,29,34] The divergences among different experiments and the differences between the results of simulations and experiments indicate that the phase transition of iron under high-strain-rate dynamic loading warrants further exploration. In this study, we use laser-induced shock loading with *in situ* x-ray diffraction technique to compress polycrystalline iron along the Hugoniot and to explore its structure and EOS in a pressure range of 9.8–88.6 GPa.

2. Experiments

The experiments were performed at the SG-Ⅱ high-power laser facility of the National Laboratory on High Power Laser and Physics.[35] A polycrystalline iron sample with a thickness of 20 μm from Goodfellow (99.9% purity) was directly irradiated by a laser beam, which was smoothed by lens array[36] and had a 450-μm-diameter focal spot. The expansion of the laser-ablated plasma transmitted a shock wave into the sample, which would continue to propagate in the sample even after the laser pulse finish and when this shock wave had passed through 1/4 to 1/3 of the sample, quasi-monochromatic x-rays were used to probe the structure of the compressed sample. The x-rays were generated by another laser beam illuminating an 8-μm-thick iron foil at an irradiance of about 1.5×10^{15} W/cm^2 and a photon energy of 6.7 keV with a bandwidth of $\sim 1\%$.

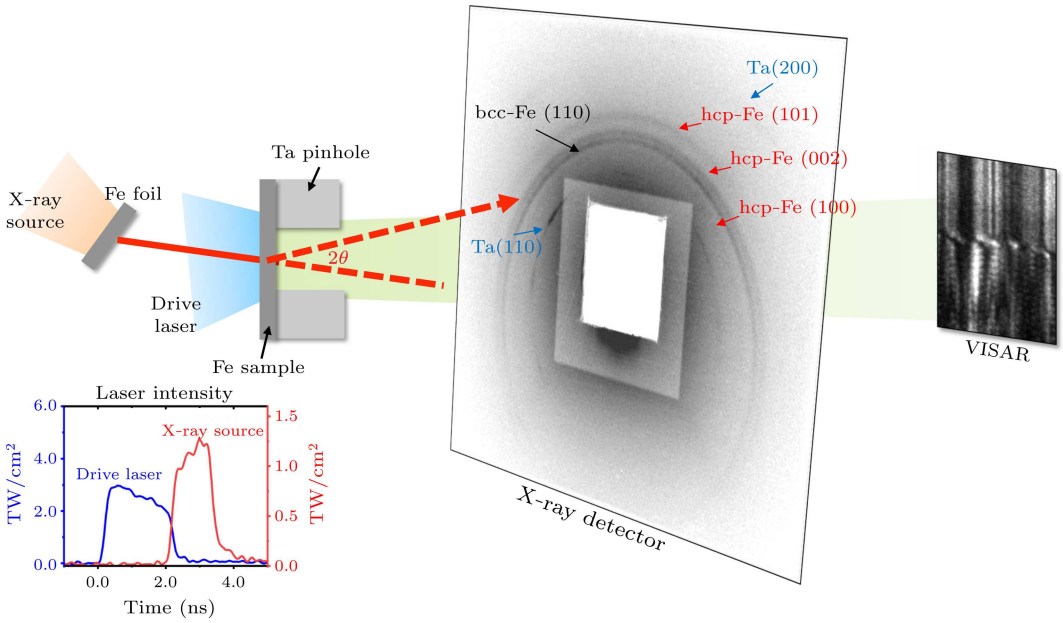


Fig. 1. Experimental setup for x-ray diffraction. A laser beam (blue) irradiates the polycrystalline iron sample so that a shock wave is transmitted into it, bringing the sample to a high-pressure and high-temperature state. Another laser beam (orange) irradiates the iron foil after a delay time to produce a quasi-monochromatic x-ray source (the laser-pulse profiles and delay times are shown in the lower-left illustration). The x-ray is collimated by the tantalum pinhole, and the Debye–Scherrer rings are recorded on the image plate (IP) in the target box. The free-surface velocity (U_{fs}) of the sample is measured by VISAR to determine the pressure state inside the sample.

A tantalum pinhole with a diameter of 300 μm mounted on the sample was used to collimate the x-rays. The Debye Scherrer diffraction rings of the sample from the center of the focal spot, which is about 300 μm in size (transverse direction), were recorded by FUJI-BAS SR image plates (IPs) lining the walls of the target box, and the lattice structure in all depth within this area will contribute to the diffraction. A 20-μm-thick iron filter covering the IPs was used to shield the high-energy x-rays and reduce the background. A typical diffraction pattern on an IP is shown in Fig. 1. This contains multiple diffraction rings from the pinhole and the ambient and shock-compressed sample; diffraction lines from the unshocked sample and pinhole edges were used as references to precisely calibrate the position of the IP plate relative to the sample and the x-ray source. The d spacings were measured via diffraction angles using the Bragg equation. The density of the compressed polycrystalline iron was determined from the unit-cell volume from the measured d spacings of the corresponding crystal structure. The main sources of uncertainty in density were the uncertainty of measured diffraction angles and the uncertainty of the x-ray wavelength. The uncertainty of the diffraction angles mainly arose from Gaussian fitting

and the oblique effect of the x-ray source and pinhole.[37] The x-ray wavelength and its uncertainty were obtained by measuring the spectrum with a bent crystal spectrometer, which gave the value as $\lambda = 1.851 \pm 0.011$ Å.

A velocity interferometer system for any reflector (VISAR)[38] was used to measure the free-surface velocity profile of the sample. According to the Rankine–Hugoniot jump condition[39] and the known polycrystalline iron Hugoniot,[21,40] the peak pressure of the sample can be obtained as $P = 1/2\rho_0 D U_{\rm fs}$, where P is the peak pressure of the sample, ρ_0 is the initial density of the sample, D is the shock-wave velocity, and $U_{\rm fs}$ is the free-surface velocity. A typical VISAR stripe image is shown on the far right of Fig. 1. The uncertainty in the measured pressure mainly arose from the uncertainty in the EOS of the sample material and uncertainty in the measured velocity from the VISAR.[37]

3. Results and discussion

A series of experiments was carried out in which polycrystalline iron was shock compressed over the range from 9.2 GPa to 88.6 GPa. In Figs. 2(a), 2(c), 2(e), and 2(g), the diffraction data from the IPs at selected pressures have been projected into 2θ–φ space, where 2θ is the diffraction angle and φ is the azimuthal angle around the direct transmitted beam. Figures 2(b), 2(d), 2(f), and 2(h) show one-dimensional diffraction patterns from selected regions of these images. Considering the non-uniformity of pressure and temperature in the sample, as well as the background formed by a large amount of stray x-rays in the dynamic compression experiments, we did not perform Rietveld refinement.

The observed diffraction lines shown in Fig. 2 come from three main sources: (1) ambient-pressure polycrystalline iron from the unshocked region of the sample, which is about 300 μm in transverse direction and 5–10 μm in longitude direction, marked by the black solid line; (2) ambient-pressure tantalum (from the pinhole edge), marked by the black dashed line; and (3) shock-compressed polycrystalline iron, which is about 300 μm in transverse direction and 10–15 μm in longitude direction, marked by short upper and lower red solid lines to avoid obscuring the signal. The diffraction geometry, such as the relative position between the sample, x-ray source, and IP, can be precisely calibrated using the ambient-pressure diffraction lines from tantalum and unshocked iron.

Figures 2(a) and 2(b) show diffraction images obtained by experiments at ambient pressure. These contain three diffraction peaks corresponding to the bcc (110) and bcc (200) planes of the tantalum pinhole and the bcc (110) plane of the unshocked iron. As mentioned above, the x-ray burst was timed so that the sample was probed while the shock wave was propagating through the iron sample but not to the free surface. As such, the ambient-pressure diffraction lines can be seen in every single shot, and their peak positions do not change within experimental uncertainty, as shown in Figs. 2(c), 2(e), and 2(g).

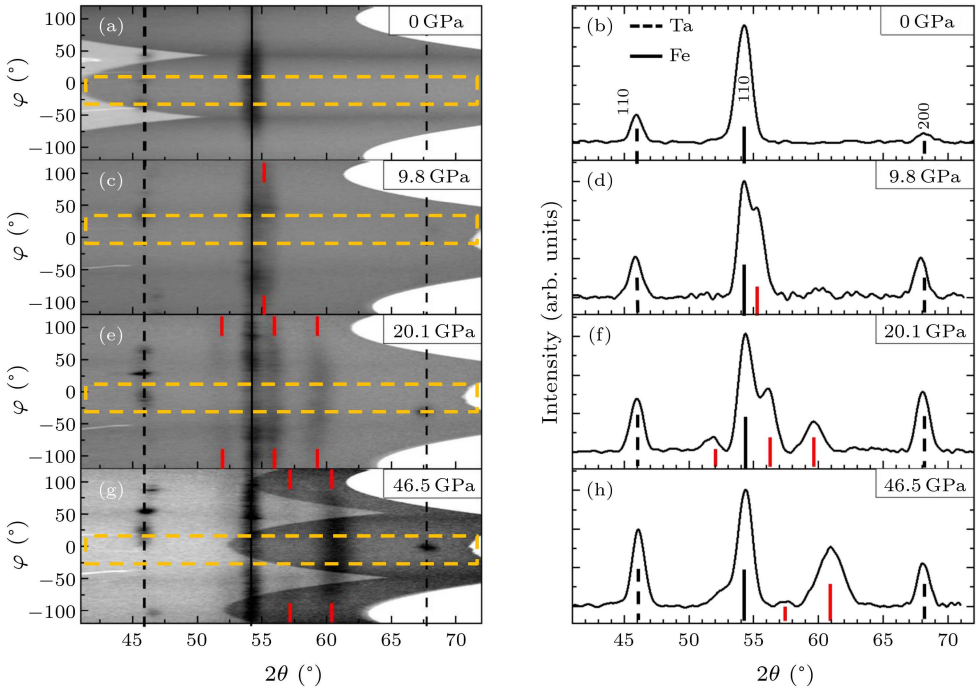


Fig. 2. Representative x-ray diffraction data for shock-compressed polycrystalline iron projected into 2θ–φ space [(a), (c), (e), (g)]. In the 2θ–φ space, diffraction peaks are straight lines of constant 2θ. The black dashed lines show the diffraction peaks from the tantalum pinhole, and the black solid lines indicate the diffraction peaks from the ambient-pressure iron sample. [(b), (d), (f), (h)] The corresponding one-dimensional x-ray diffraction patterns for the selected regions defined by the yellow dashed lines in the corresponding left panels.

Figures 2(c) and 2(d) show diffraction images of polycrystalline iron under a shock pressure of 9.8 GPa. In addition to the ambient-pressure diffraction lines as seen in Figs. 2(a) and 2(b), a new peak next to the iron bcc (110) peak can be seen. To identify to which crystal structure this new peak belongs, in Fig. 3, measured d spacings are plotted as a function of pressure alongside extrapolations for three candidate phases of iron (fcc, hcp, and bcc)[15,16,41] using the third-order Birch–Murnaghan EOS. As can be seen, this new diffraction peak does not match any of the three d spacings of fcc, but it is close to bcc (110) and hcp (002). Further analysis shows that the diffraction peak corresponds to the compressed bcc (110) plane of polycrystalline iron. There are two main reasons for this. First, in the hcp crystal structure, the diffraction intensity of the hcp (101) peak is stronger than that of the hcp (002) peak. If the new peak corresponds to hcp (002), the hcp (110) peak is expected to appear and will have a higher intensity, as shown in Figs. 2(e) and 2(g). However, there are no similar characteristics in Fig. 2(c), which means that the new peak should come from compressed bcc (110). Second, the density calculated using the P–ρ relationship of polycrystalline iron along the Hugoniot at 9.8 GPa is 8.26 g/cm^3. This is in a good agreement with the density deduced from the compressed bcc (110) d spacing, with a difference within 1%. In contrast, a large density jump of more than 5% will occur if the new peak is hcp (002). Therefore, we suggest that at 9.8 GPa, the polycrystalline iron has not undergone a phase transition and still has a completely bcc structure.

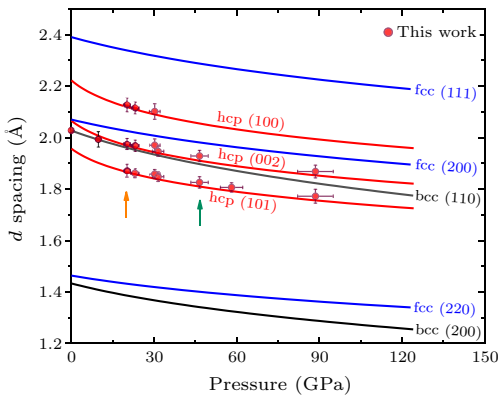


Fig. 3. Measured d spacings of polycrystalline iron as a function of pressure. The red circles are the experimental data obtained in this work, and the orange and green arrows point to d spacings under pressures of 20.1 GPa and 46.5 GPa, respectively. The data for the bcc structure (black line) and the hcp structure (red line) were derived from diamond anvil cell experiments and their extrapolations at 300 K,[15,16] and the fcc structure was derived from the density functional theory simulations at 0 K.[41]

There are three new diffraction peaks at 20.1 GPa, as shown in Figs. 2(e) and 2(f). These three diffraction peaks agree very well with the (100), (002), and (101) reflections of the hcp structure, which is shown by the orange arrow in Fig. 3. It is clear that the polycrystalline iron has undergone a martensitic transformation from a bcc to an hcp crystal structure. It is generally believed that in a martensitic transition, the new phase is derived from the parent phase through collective shear motion of atomic planes, resulting in a unique crystal orientation relationship between the two phases. As for the iron phase transition presented here, a two-step process mechanism is widely accepted. Firstly, the (001) crystal planes of the bcc iron are compressed and expand along the $(1\bar{1}0)$ direction, so the bcc (110) planes become hexagonally arranged planes, corresponding to the (0002) planes in the hcp structure. Subsequently, the alternate (110) planes move along the $(1\bar{1}0)$ direction, while the interplane distance d(110) remains unchanged, forming the hcp structure. Therefore, the orientation relationships between the new phase and the parent phase are hcp(0002)$\|$bcc(110) and hcp$(0\bar{1}10)\|$bcc$(1\bar{1}0)$.

Since the d spacings of hcp (002) and bcc (110) are very close at this pressure, it is difficult to determine whether the hcp (002) peak is mixed up with the compressed bcc (110) peak. Meanwhile, the diffraction angle corresponding to the bcc (200) plane is beyond the experimental observation range due to our diffraction geometry. It is thus difficult to determine whether there is two-phase coexistence using the diffraction images alone. Further analysis was therefore conducted to compare the sample density inferred from the measured d spacings and the P–ρ relationship along the Hugoniot. The density deduced from unit cell of the hcp phase of iron is 9.04 g/cm^3, and the value corresponding to the bcc structure is 8.54 g/cm^3. This means that the density of a compressed sample containing both bcc and hcp structures should be between 8.54 g/cm^3 and 9.04 g/cm^3. The density calculated using the P–ρ relationship along the iron Hugoniot is 9.07 g/cm^3, which is very close to the hcp density, indicating that the sample has an almost entirely hcp crystal structure, and there is no two-phase coexistence at 20.1 GPa.

Figures 2(g) and 2(h) show diffraction images at 46.5 GPa, in which three new diffraction peaks can be seen. However, the diffraction peak of hcp (100) cannot be used to obtain an accurate diffraction angle due to its low signal-to-noise ratio (SNR). The other two diffraction peaks are in good agreement with the hcp structure, and bcc (110) and hcp (002) peaks can be clearly distinguished at this pressure, as shown by the green arrow in Fig. 3. If the diffraction angle $2\theta = 60.9°$ corresponds to the hcp (002) peak, then the density of the sample is 9.70 g/cm^3, which is very close to the Hugoniot density (9.73 g/cm^3). Conversely, if the diffraction angle comes from the bcc (110) peak, the density will have a large jump of more than 6%. Therefore, at 46.5 GPa, the polycrystalline iron has completed the phase transition and become a completely hcp structure. Based on the same analysis process, we believe that polycrystalline iron maintains an hcp crystal structure up to 88.6 GPa, which was the maximum pressure

in our experiments. Based on the d spacings and relative intensities of diffraction lines, as well as the calculated densities, the hcp structure provides the most consistent explanation for our observed data at 20.1 GPa and above. It should be noted that the SNR gradually deteriorates with increasing pressure, which may be brought by the stronger plasma plume from samples, and ultimately resulting in a failure to obtain effective dynamic-diffraction results.

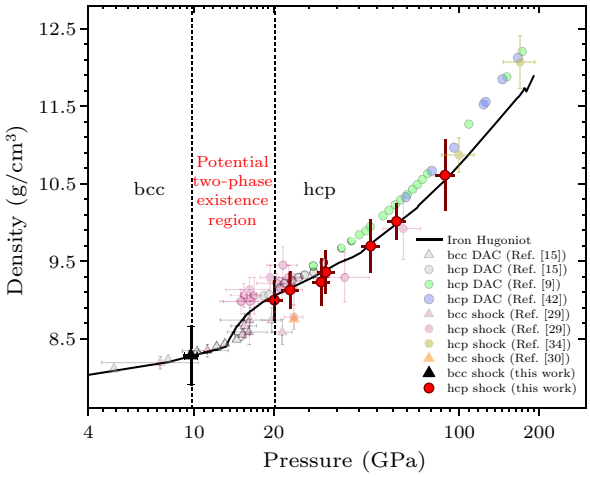


Fig. 4. Plot of density vs. pressure for shock-compressed polycrystalline iron. The pressure was interpreted from free-surface velocity measurements made by VISAR, and the density was measured using x-ray diffraction. The bcc structures are marked with triangles and the hcp structures are marked with circles. The light-colored data are from XRD measurements in the literature,[9,15,29,30,34,42] and the dark-color data are the results from this work. The gas-gun Hugoniot is plotted as the solid black line.[21,40] Our data agree very well with the gas-gun Hugoniot. As can be seen, there are only bcc phases at 9.8 GPa and only hcp phases at 20.1 GPa. The potential co-existing pressure range of the two phases is thus between 9.8 GPa and 20.1 GPa.

Figure 4 shows a plot of the density as a function of pressure (as deduced from the VISAR data) for both iron phases, along with the gas-gun Hugoniot. It can be seen that our data, which was obtained from laser-shocked polycrystalline iron, agrees very well with the gas-gun Hugoniot within the pressure range of the experiments (9.8–88.6 GPa). Compared with the static-compression data, our shock-compression data shows lower densities at any given pressure. This hardening response may result from the rapidly increasing internal temperature and intense interatomic motion in the material due to shock loading, which becomes stronger with increasing pressure. As we know, in the static compression experiments, the sample system is in a thermal equilibrium state with the outside environment, makes the temperature almost constant, in contrast, dynamic compression drives the sample into a non-equilibrium adiabatic state, and the temperature rises rapidly with the heating of the sample by plastic work of the shock wave. Therefore, there may be a large uncertainty when extrapolating static-compression data to infer the experimental results under dynamic loading.

It can be seen in Fig. 4 that no two-phase coexistence was observed in our experiments. We thus speculate that the pressure of complete phase transition should not exceed 20.1 GPa, which is different from the experimental results of Hawreliak *et al.*[29] In their experiments, the bcc phase was found to still exist at about 30 GPa. In contrast, our results are consistent with those of Mathon *et al.*,[32] who found that the phase transition was completed at a pressure of $\sim$ 16.2 GPa. There may be many factors affecting the measured starting and ending pressures of the phase transition, including the uniformity of the pressure in the sample, the loading strain rate, and the initial structure of the sample. The accurate pressure range of the phase transition in polycrystalline iron under shock loading needs to be further verified by a more targeted experimental design and more stable pressure control.

4. Conclusion

In this work, we have investigated the lattice-compression and phase-transition behavior of shock-compressed polycrystalline iron by combining macro- and microscopic diagnoses at the SG-Ⅱ high-power laser facility. The *in situ* XRD results show that the initial polycrystalline iron has a bcc structure. With increasing pressure, this bcc lattice structure is first compressed and then changes to an hcp structure. The data from this work show good agreement with the gas-gun Hugoniot, but do not agree well with static-compression experiments. This indicates that there may be a problem with extrapolating from static-compression data to predict the dynamic responses of materials at extremely high pressures. We did not find evidence of an fcc structure, as has been predicted by molecular dynamics simulations for shocked polycrystalline iron. This is because the fcc structure is a transient metastable phase, and there are magnitude differences in terms of time scale and strain rate between the experiments and simulations. In addition, no coexistence of the bcc and hcp phases was found in the range of experimental pressures, indicating that the bcc structure has been completely transformed into an hcp structure at 20.1 GPa, which is consistent with the phase transition pressure interval of 13.8–16.2 GPa proposed by Mathon *et al.*[32] Further experimental verification is needed to obtain a more accurate pressure range for the phase transition. The ability to use *in situ* x-ray diffraction to directly observe the lattice compression and phase transformation of polycrystalline iron during shock compression offers the potential to deepen the understanding of the dynamic response characteristics of materials under extreme conditions.

Acknowledgments

The authors are grateful to the SG-Ⅱ laser operation group for their laborious work and close collaboration. This work was supported by the National Natural Science Foundation of China (Grant Nos. 12304033, 12072328, and 11991073).

References

[1] Birch F 1952 *J. Geophys. Res.* **57** 227
[2] Hemley R J and Mao H K 2001 *Int. Geol. Rev.* **43** 1
[3] Birch F 1961 *Geophys. J. R. Astron. Soc.* **4** 295
[4] Kerley G I 1993 *Multiphase equation of state for iron*, Sandia National Lab. (SNL-NM), Albuquerque, NM (United States)
[5] Batani D, Morelli A, Tomasini M, Benuzzi-Mounaix A, Philippe F, Koenig M, Marchet B, Masclet I, Rabec M and Reverdin C 2002 *Phys. Rev. Lett.* **88** 235502
[6] Dewaele A, Loubeyre P, Occelli F, Mezouar M, Dorogokupets P I and Torrent M 2006 *Phys. Rev. Lett.* **97** 215504
[7] Weng Y, Dong H and Gan Y 2011 *Advanced steels: the recent scenario in steel science and technology* (Berlin: Springer Science & Business Media) p. 15
[8] Hosford W F 2012 *Iron and steel* (Cambridge: Cambridge University Press) p. 195
[9] Sakai T, Takahashi S, Nishitani N, Mashino I, Ohtani E and Hirao N 2014 *Phys. Earth Planet. Interiors* **228** 114
[10] Fischer R A and Campbell A J 2015 *Am. Mineral.* **100** 2718
[11] Sakamaki T, Ohtani E, Fukui H, Kamada S, Takahashi S, Sakairi T, Takahata A, Sakai T, Tsutsui S and Ishikawa D 2016 *Sci. Adv.* **2** e1500802
[12] Sundaram V 1996 *Bull. Mater. Sci.* **19** 1025
[13] Manes A, Serpellini F, Pagani M, Saponara M and Giglio M 2014 *Int. J. Impact Eng.* **69** 39
[14] Bancroft D, Peterson E L and Minshall S 1956 *J. Appl. Phys.* **27** 291
[15] Mao H K, Bassett W A and Takahashi T 1967 *J. Appl. Phys.* **38** 272
[16] Mao H K, Wu Y, Chen L C, Shu J F and Jephcoat A P 1990 *J. Geophys. Res.* **95** 21737
[17] Funamori N, Yagi T and Uchida T 1996 *Geophys. Res. Lett.* **23** 953
[18] Rueff J P, Krisch M, Cai Y Q, Kaprolat A and Sette F 1999 *Phys. Rev. B* **60** 14510
[19] Barker L M and Hollenbach R E 1974 *J. Appl. Phys.* **45** 4872
[20] Brown J M and McQueen R G 1986 *J. Geophys. Res.: Solid Earth* **91** 7485
[21] Boettger J C and Wallace D C 1997 *Phys. Rev. B* **55** 2840
[22] Hawreliak J, Colvin J D, Eggert J H, Kalantar D H, Lorenzana H E, Stölken J S, Davies H M, Germann T C, Holian B L, Kadau K, Lomdahl P S, Higginbotham A, Rosolankova K, Sheppard J and Wark J S 2006 *Phys. Rev. B* **74** 184107
[23] Remington T P, Remington B A, Hahn E N and Meyers M A 2017 *Mater. Sci. Eng. A* **688** 429
[24] Jensen B J, Gray G T and Hixson R S 2009 *J. Appl. Phys.* **105** 103502
[25] Wang J, Smith R F, Eggert J H, Braun D G, Boehly T R, Reed Patterson J, Celliers P M, Jeanloz R, Collins G W and Duffy T S 2013 *J. Appl. Phys.* **114** 023513
[26] Azarevich A, Bolotina N, Khrykina O, Bogach A, Zhukova E, Gorshunov B, Melentev A, Bedran Z, Alyabyeva A, Belyanchikov M, Voronov V, Shitsevalova N Y, Filipov V B and Sluchanko N 2022 *Chin. Phys. Lett.* **39** 127302
[27] Li X, Ding B, Feng Y, Wu R, Tian L, Huang J and Liu X 2022 *Chin. Phys. Lett.* **39** 033401
[28] Kalantar D H, Belak J F, Collins G W, Colvin J D, Davies H M, Eggert J H, Germann T C, Hawreliak J, Holian B L, Kadau K, Lomdahl P S, Lorenzana H E, Meyers M A, Rosolankova K, Schneider M S, Sheppard J, Stolken J S and Wark J S 2005 *Phys. Rev. Lett.* **95** 075502
[29] Hawreliak J A, El-Dasher B, Lorenzana H, Kimminau G, Higginbotham A, Nagler B, Vinko S M, Murphy W J, Whitcher T, Wark J S, Rothman S and Park N 2011 *Phys. Rev. B* **83** 144114
[30] Li J, Chen X H, Wu Q, Luo B Q, Li M, Yang Q G, Tao T J, Jin K, Geng H Y, Tan Y and Xue T 2017 *Acta Phys. Sin.* **66** 136101 (in Chinese)
[31] Wang F M and Ingalls R 1998 *Phys. Rev. B* **57** 5647
[32] Mathon O, Baudelet F, Itie J P, Polian A, d'Astuto M, Chervin J C and Pascarelli S 2004 *Phys. Rev. Lett.* **93** 255503
[33] Kadau K, Germann T C, Lomdahl P S, Albers R C, Wark J S, Higginbotham A and Holian B L 2007 *Phys. Rev. Lett.* **98** 135701
[34] Denoeud A, Ozaki N, Benuzzi-Mounaix A, *et al.* 2016 *Proc. Natl. Acad. Sci. USA* **113** 7745
[35] Lin Z, Deng X, Fan D, Wang S, Chen S, Zhu J, Qian L, Shen X, Xu F and Zhu J 1999 *Fusion Eng. Des.* **44** 61
[36] Deng X, Liang X, Chen Z, Yu W and Ma R 1986 *Appl. Opt.* **25** 377
[37] Rygg J R, Smith R F, Lazicki A E, Braun D G, Fratanduono D E, Kraus R G, McNaney J M, Swift D C, Wehrenberg C E, Coppari F, Ahmed M F, Barrios M A, Blobaum K J M, Collins G W, Cook A L, Di Nicola P, Dzenitis E G, Gonzales S, Heidl B F, Hohenberger M, *et al.* 2020 *Rev. Sci. Instrum.* **91** 043902
[38] Celliers P M, Bradley D K, Collins G W, Hicks D G, Boehly T R and Armstrong W J 2004 *Rev. Sci. Instrum.* **75** 4916
[39] Duvall G E and Graham R A 1977 *Rev. Mod. Phys.* **49** 523
[40] Brown J M, Fritz J N and Hixson R S 2000 *J. Appl. Phys.* **88** 5496
[41] Alnemrat S, Hooper J P, Vasiliev I and Kiefer B 2014 *J. Phys.: Condens. Matter* **26** 046001
[42] Antonangeli D, Morard G, Paolasini L, Garbarino G, Murphy C A, Edmund E, Decremps F, Fiquet G, Bosak A, Mezouar M and Fei Y 2018 *Earth Planet. Sci. Lett.* **482** 446